Probabilistic Engineering Mechanics 53 (2018) 75–86

Contents lists available at ScienceDirect

Probabilistic Engineering Mechanics

journal homepage: www.elsevier.com/locate/probengmech

Adaptive sub-interval perturbation-based computational strategy for epistemic uncertainty in structural dynamics with evidence theory

Dawei Li [a], Hesheng Tang [a,*], Songtao Xue [a], Yu Su [b]

[a] State Key Laboratory for Disaster Reduction in Civil Engineering, Tongji University, 1239, Siping Rd., Shanghai, China
[b] School of Civil Engineering, Architecture and Environment, Hubei University of Technology, 28, Nanli Rd, Wuhan, China

ARTICLE INFO

Keywords:
Structural dynamic problem
Evidence theory
Uncertainty quantification
Adaptive sub-interval perturbation method

ABSTRACT

Evidence theory, with its powerful features for uncertainty analysis, provides an alternative to probability theory for representing epistemic uncertainty, which is an uncertainty in a system caused by the impreciseness of data or knowledge that can be conveniently addressed. However, this theory is time-consuming for most applications because of its discrete property. This article describes an adaptive sub-interval perturbation-based computational strategy for representing epistemic uncertainty in structural dynamic analysis with evidence theory. The possibility of adopting evidence theory as a general tool for uncertainty quantification in structural transient response under stochastic excitation is investigated using an algorithm that can alleviate computational difficulties. Simulation results indicate that the effectiveness of the presented strategy can be used to propagate uncertainty representations based on evidence theory in structural dynamics.

1. Introduction

Deterministic analysis and design result may not afford resident loss because of the implication of inherent uncertainty in structural systems and ground motion. This condition causes researchers to consider the uncertainty effects of earthquake response on structural systems. Engineering uncertainties are classified into aleatory and epistemic according to the nature of uncertain sources [1,2]. Aleatory uncertainty stems from sources that are inherently random (or aleatory) in engineering or scientific analysis (e.g., properties of non-uniform materials, manufacturing tolerance, and environmental effects). Epistemic uncertainty results from incomplete knowledge, ignorance, or modeling (e.g., simplification of mathematical models of buildings for structural analysis). In the preliminary stage of uncertainty quantification (UQ), the randomness of significant loads (e.g., earthquake, wind, and wave.) has received considerable attention and has been modeled by non-stationary stochastic processes with good accuracy. Subsequently, the stochastic response of a deterministic system under random loads is investigated using the well-established random vibration theory [3–5]. However, as described earlier, not only excited loads demonstrate uncertainty, but also structural systems. Compared with the randomness of excited loads, the uncertainty of structural systems is always epistemic due to incomplete knowledge, ignorance, or modeling.

Probability theory, as a classical UQ theory, has been prevalently implemented to evaluate the uncertain response of dynamic systems with uncertain parameters [6]. Preliminary random structural analysis directly combines the Monte Carlo (MC) sampling method with structural dynamic analysis to compute the uncertain response of a system [7]. To overcome the high computational cost of brute-force MC simulation, the spectral method [8,9], perturbation method [10] and its advanced versions [11], probability density evolution method [12], random factor method [13], and dynamic variability response functions [14,15] are implemented in the probabilistic finite element method.

In contrast to the main assumption of classical probability theory, the perfect knowledge of distribution type and the large amount of statistical data required to determine the true value of distribution parameters, real statistical data, and pre-knowledge of uncertainty inherent in a structural system and environment are always imperfect or unavailable. This scenario clearly suggests that probability theory is excessively optimistic but cannot sufficiently emphasize extremes or epistemic uncertainty. Alternatively, epistemic UQ techniques have been investigated to model imprecise, vague, fuzzy, ambiguous, and incomplete variabilities involved in engineering. The most representative theories are fuzzy set theory [16], possibility theory [17], interval analysis [18], imprecise probability theory [19] and evidence theory [20,21]. Compared with other theories [22], evidence theory has the most potential benefit because it has the least restrictive representation framework for aleatory and epistemic uncertainties. Evidence theory is widely used

* Corresponding author.
E-mail address: thstj@tongji.edu.cn (H. Tang).

https://doi.org/10.1016/j.probengmech.2018.05.001
Received 6 September 2017; Received in revised form 9 April 2018; Accepted 8 May 2018
Available online 26 May 2018

in uncertainty reasoning, data fusion, and decision-making given its combination rule feature for different uncertainty sources [23].

Although evidence theory has been successfully applied to scientific analysis and to certain engineering practices, its drawbacks should be considered. As a promising advantage of evidence theory, uncertain information is flexibly represented by a series of discrete intervals, which result in an extreme computational demand in uncertainty propagation and challenges in its application in complex and large-scale engineering problems. Potential approaches, such as the revised multi-point approximation [24], combination of Latin hypercube sampling and nonparametric regression-based response surface approximations [25], radial basis function-based surrogate model [26], intelligent optimization algorithm [27], and point-collection method [28], have been developed to improve the practical application of evidence theory in the last decades, thereby successfully alleviating the excessive computational costs of large-scale applications and the repetitive simulations required for evidential uncertainty propagation.

Despite the enthusiasm for static or quasi-static problem, the aforementioned methods will result in considerable computational and time costs in history analysis. When the computational burden involved in a time-variant dynamic system is considered, the perturbation method combined with precise time integration is adopted to handle the slight fluctuation of uncertain variables in an uncertain dynamic system [29,30]. Representative investigations in this area have been explored. For example, Rao et al. [31] used the adaptive Taylor first-order expansion and direct optimization, which combines the interval finite element approach and fuzzy formalism to obtain the transient response of the structure with uncertain parameters. Muscolino et al. [32,33] extended first-order perturbation with affine arithmetic to cope with upper and lower bound structural dynamic responses under stationary and non-stationary excitations with a slight fluctuation in uncertain structural parameters. Qiu et al. [34] proposed sub-interval measures to enhance the capability for addressing large uncertainty levels in perturbation analysis. Zhou et al. [35] introduced the sub-interval methodology into interval perturbation to deal with large uncertainties in an uncertain system. Xia et al. used sub-interval and modified sub-interval perturbations to quantify the uncertainty in the static response analyses of structures [36] and structural–acoustic systems [37], respectively. Wang et al. [38] proposed two types of sub-interval perturbation method (SPM) to solve the problem of uncertain heat conduction with large fuzzy parameters. Yin et al. [39] implemented SPM into UQ for mid-frequency analysis with evidence theory. Despite several preliminary studies on SPM in static problems, SPM-based evidential UQ in structural dynamic problems has not yet been explored.

The application of SPM-based evidential UQ to structural dynamics problems appears interesting and promising based on the characteristics of such problems. However, the computational accuracy of classical SPM is improved by sacrificing computational efficiency due to the use of a crude mesh for sub-intervals in perturbation, which leads to an exponential increase in computational cost. To alleviate the computational consumption of classical SPM in non-probabilistic uncertainty analysis, a sensible adaptive strategy is proposed in this work to reduce the dimensions of a system with uncertain input and to construct a reasonable combination of sub-intervals in the joint focal element.

The remaining parts of this paper are organized as follows. Section 2 presents an evidential UQ framework for investigating the variance of the displacement response of a dynamic system under stochastic excitation. Section 3 explains the adaptive sub-interval perturbation method (ASPM)-based uncertainty propagation in UQ of the structural transient response under stochastic excitation. Section 4 provides the uncertainty measurement for the transient response of a dynamic system. Section 5 summarizes the evidential UQ framework with ASPM. Two illustrative examples are presented in Section 6 to investigate the effectiveness and accuracy of the proposed method. Section 7 provides the conclusion of this work.

2. Epistemic uncertainty represented by evidence theory in a dynamic system under stochastic excitation

Without losing generality, the motion equation of a multiple degree of freedom system (MDOF) under nonstationary random excitation is expressed as

$$\mathbf{M}(\boldsymbol{\alpha})\ddot{\mathbf{u}}(\boldsymbol{\alpha},\boldsymbol{\omega},t)+\mathbf{C}(\boldsymbol{\alpha})\dot{\mathbf{u}}(\boldsymbol{\alpha},\boldsymbol{\omega},t)+\mathbf{K}(\boldsymbol{\alpha})\mathbf{u}(\boldsymbol{\alpha},\boldsymbol{\omega},t)=\mathbf{f}(\boldsymbol{\alpha},\boldsymbol{\omega},t), \tag{1}$$

where $\mathbf{M}(\boldsymbol{\alpha})$, $\mathbf{C}(\boldsymbol{\alpha})$, and $\mathbf{K}(\boldsymbol{\alpha})$ respectively denote the mass, damping, and stiffness matrices of a structural system with $\Gamma\times\Gamma$ elements. $\ddot{\mathbf{u}}(\boldsymbol{\alpha},\boldsymbol{\omega},t)$, $\dot{\mathbf{u}}(\boldsymbol{\alpha},\boldsymbol{\omega},t)$ and $\mathbf{u}(\boldsymbol{\alpha},\boldsymbol{\omega},t)$ are the vectors of acceleration, velocity, and displacement, respectively, of a structural system. $\mathbf{f}(\boldsymbol{\alpha},\boldsymbol{\omega},t)$ is zero-mean-valued nonstationary random excitation vector with $\Gamma\times 1$ elements. The parameter collection $\boldsymbol{\alpha}=\left[\alpha_1,\alpha_2,\ldots,\alpha_N\right]^{\mathrm{T}}$ is used to characterize the mutually independent uncertain parameters of a structural system, where N denotes the number of parameters of a structural system with epistemic uncertainty and the symbol T denotes the transpose operator of the matrix. Based on the concept of pseudo-excitation method [3,5], the random excitation $\mathbf{f}(\boldsymbol{\alpha},\boldsymbol{\omega},t)$ can be rewritten as a series of pseudo harmonic excitations:

$$\mathbf{f}(\boldsymbol{\alpha},\boldsymbol{\omega},t)=\sum_{g=1}^{G}\mathrm{vec}\left(\mathbf{M}(\boldsymbol{\alpha})\mathbf{E}_m\sqrt{S(\omega_g,t)}\exp(i\omega_g t)\right) \tag{2}$$

where $\mathbf{E}_m$ is the identity matrix; $S(\omega_g,t)$ is the component of time variant power spectral density $\mathbf{S}(\boldsymbol{\omega},t)$; G is the number of discrete frequency intervals and $i=\sqrt{-1}$ is the imaginary unit. The response statistics for the displacement $u_\tau(\boldsymbol{\alpha},\boldsymbol{\omega},t)$, $\tau\in\forall[1,\Gamma]$ is considered as the response quantities of interest. The time variant power spectral density of $u_\tau(\boldsymbol{\alpha},\boldsymbol{\omega},t)$ is given as:

$$\mathbf{S}_{u_\tau u_\tau}(\boldsymbol{\alpha},\boldsymbol{\omega},t)=u_\tau^*(\boldsymbol{\alpha},\boldsymbol{\omega},t)\,u_\tau(\boldsymbol{\alpha},\boldsymbol{\omega},t) \tag{3}$$

where $*$ indicates the complex conjugate operator. Then, the auto-covariance function of $u_\tau(\boldsymbol{\alpha},\boldsymbol{\omega},t)$ can be depicted as the product of an integration in the frequency field:

$$D_{u_\tau u_\tau}(\boldsymbol{\alpha},t)=2\times\Delta\omega\sum_{g=1}^{G}u_\tau^*(\boldsymbol{\alpha},\omega_g,t)\,u_\tau(\boldsymbol{\alpha},\omega_g,t)\quad\tau\in\forall[1,\Gamma], \tag{4}$$

The Eq. (4) shows that the uncertainties of $D_{u_\tau u_\tau}(\boldsymbol{\alpha},t)$ is dependent on the uncertain structural parameter vector $\boldsymbol{\alpha}$. Therefore, the probabilistic result of $D_{u_\tau u_\tau}(\boldsymbol{\alpha},t)$ is conditioned by precise probabilistic model of uncertain parameters $\boldsymbol{\alpha}$. By contrast, the fragment and incomplete uncertain information of $\boldsymbol{\alpha}$ will produce epistemic UQ results of $D_{u_\tau u_\tau}(\boldsymbol{\alpha},t)$.

Evidence theory [20,21] is used in this study to address epistemic uncertainty involved in structural parameters. In [20,21], the evidential expression of each component α_n ($n\in\forall[1,N]$) in the uncertain structural property vector $\boldsymbol{\alpha}$ is built as the combination of focal element α_n^{I} and the corresponding basic belief assignment (BBA) m_{n,j_n} as follows:

$$\left\{\boldsymbol{\alpha}_{n,j_n}^{\mathrm{I}},m_{n,j_n}\right\}=\left\{\left[\underline{\alpha}_{n,j_n},\bar{\alpha}_{n,j_n}\right],m_{n,j_n}\right\}\quad j_n\in\forall[1,J_n]\quad n\in\forall[1,N], \tag{5}$$

where $\underline{\alpha}_{n,j_n}$ and $\bar{\alpha}_{n,j_n}$ are the lower and upper bounds, respectively, of the j_nth focal element $\alpha_{n,j_n}^{\mathrm{I}}$ of the uncertain component α_n; and J_n is the number of focal element of α_n. As the basic measure in evidence theory, the BBA m_{n,j_n} express the degree of assignment belief of a proposition and satisfy with followings:

$$\begin{cases}m_{n,j_n}\geq 0 & \boldsymbol{\alpha}_{n,j_n}^{\mathrm{I}}\subset\Omega\quad\text{and}\quad\boldsymbol{\alpha}_{n,j_n}^{\mathrm{I}}\in\Theta\\ m_{n,j_n}=0 & \boldsymbol{\alpha}_{n,j_n}^{\mathrm{I}}\subset\Omega\quad\text{and}\quad\alpha_{n,j_n}^{\mathrm{I}}\in\Theta\end{cases}, \tag{6}$$

$$\sum m_{n,j_n}=1\;\alpha_{n,\quad j_n}^{\mathrm{I}}\in\Theta, \tag{7}$$

where Ω is the discernment frame used to denote the entire collection of mutually exclusive and exhaustive possible elementary propositions in evidence theory, and $\Theta=2^{\Omega}$ is the countable power set to support BBA as a mapping, $m:\Theta\rightarrow[0,1]$, for a meaningful proposition. When evidence theory is used to model the uncertain parameter vector $\boldsymbol{\alpha}$, the

uncertain input of system function is built by the Cartesian product as follows:

$$\left\{\boldsymbol{\alpha}_q^{\mathrm{I}}, m_q\right\} = \left\{\left(\alpha_{1,j_1}^{\mathrm{I}}, m_{1,j_1}\right), \ldots, \left(\alpha_{n,j_n}^{\mathrm{I}}, m_{n,j_n}\right), \ldots, \left(\alpha_{N,j_N}^{\mathrm{I}}, m_{N,j_N}\right)\right\},$$
$$j_n \in \forall[1, J_n], n \in \forall[1, N], q \in \forall[1, \prod_{n=1}^{N} J_n], \tag{8}$$

$$m_q = \prod_{n=1}^{N} m_{n,j_n}, j_n \in \forall[1, J_n], n \in \forall[1, N], q \in \forall[1, \prod_{n=1}^{N} J_n], \tag{9}$$

where $\prod_{n=1}^{N} J_n$ is the number of joint focal elements. On the basis of the aforementioned definition, the evidential expression of $D_{u_\tau u_\tau}(\boldsymbol{\alpha}, t)$ is given as

$$\left\{\left[\underline{D}_{u_\tau u_\tau}(\boldsymbol{\alpha}_q^{\mathrm{I}}, t), \overline{D}_{u_\tau u_\tau}(\boldsymbol{\alpha}_q^{\mathrm{I}}, t)\right], m_q\right\}$$
$$= \left\{[\min\left(D_{u_\tau u_\tau}\left(\boldsymbol{\alpha}_q^{\mathrm{I}}, t\right)\right), \max\left(D_{u_\tau u_\tau}\left(\boldsymbol{\alpha}_q^{\mathrm{I}}, t\right)\right)], m_q\right\},$$
$$q \in \forall[1, \prod_{n=1}^{N} J_n], \tag{10}$$

where $\underline{D}_{u_\tau u_\tau}(\boldsymbol{\alpha}_q^{\mathrm{I}}, t)$ and $\overline{D}_{u_\tau u_\tau}(\boldsymbol{\alpha}_q^{\mathrm{I}}, t)$ are used to denote the lower and upper bounds, respectively, of $D_{u_\tau u_\tau}(\boldsymbol{\alpha}_q^{\mathrm{I}}, t)$. min(•) and max(•) represent the operators for searching for the minimum and maximum values of the investigated problems. Evidently, the computation cost of Eq. (10) is mainly dependent on the number of $\prod_{n=1}^{N} J_n$ in a given dynamic system. To alleviate the computational burden of the evidential uncertainty propagation of Eq. (10), the adaptive sub-interval strategy is introduced into the perturbation method based on the first-order Taylor expansion.

3. Evidential uncertainty propagation with adaptive strategy

Uncertainty propagation is the most critical stage of UQ. In this section, the major concepts of interval perturbation, sub-interval strategy and the adaptive dimension reduction methodology are introduced. Moreover, the numerical evaluation of ASPM is summarized.

3.1. Assessment of evidential response using the interval perturbation method

As discussed in the previous section, the propagation of $D_{u_\tau u_\tau}\left(\boldsymbol{\alpha}_q^{\mathrm{I}}, t\right)$ may result in the dimensional curse due to the increment in the number of focal elements. To alleviate computational burden, interval perturbation analysis is performed to propagate the uncertainty in $D_{u_\tau u_\tau}\left(\boldsymbol{\alpha}_q^{\mathrm{I}}, t\right)$. When a similar definition of interval perturbation analysis is adopted, $\boldsymbol{\alpha}_q^{\mathrm{c}}$ and $\Delta\boldsymbol{\alpha}_q$ are called the nominal value and deviation radius, respectively, of the joint focal element $\boldsymbol{\alpha}_q^{\mathrm{I}}$.

$$\boldsymbol{\alpha}_q^{\mathrm{c}} = \mathrm{vec}\left(\frac{\underline{\alpha}_{1,j_1} + \bar{\alpha}_{1,j_1}}{2}, \ldots, \frac{\underline{\alpha}_{n,j_n} + \bar{\alpha}_{n,j_n}}{2}, \ldots, \frac{\underline{\alpha}_{N,j_N} + \bar{\alpha}_{N,j_N}}{2}\right)$$
$$q \in \forall[1, Q] \quad j_n \in \forall[1, J_n] \quad n \in \forall[1, N], \tag{11}$$

$$\Delta\boldsymbol{\alpha}_q = \mathrm{vec}\left(\frac{\bar{\alpha}_{1,j_1} - \underline{\alpha}_{1,j_1}}{2}, \ldots, \frac{\bar{\alpha}_{n,j_n} - \underline{\alpha}_{n,j_n}}{2}, \ldots, \frac{\bar{\alpha}_{N,j_N} - \underline{\alpha}_{N,j_N}}{2}\right)$$
$$q \in \forall[1, Q] \quad j_n \in \forall\left[1, J_n\right] \quad n \in \forall[1, N], \tag{12}$$

where $\underline{\alpha}_{n,j_n}$ and $\bar{\alpha}_{n,j_n}$ are the lower and upper bounds, respectively, of component $\alpha_{n,j_n}^{\mathrm{I}}$ in joint focal element α_q^{I}; and $Q = \prod_{n=1}^{N} J_n$ is the number of joint focal elements. When the first-order Taylor series expansion is used, the values of $\underline{D}_{u_\tau u_\tau}(\boldsymbol{\alpha}_q^{\mathrm{I}}, t)$ and $\overline{D}_{u_\tau u_\tau}(\boldsymbol{\alpha}_q^{\mathrm{I}}, t)$ are given as

$$\underline{D}_{u_\tau u_\tau}\left(\boldsymbol{\alpha}_q^{\mathrm{I}}, t\right) = D_{u_\tau u_\tau}\left(\boldsymbol{\alpha}_q^{\mathrm{c}}, t\right) - \sum_{n=1}^{N}\left|\partial D_{u_\tau u_\tau}\left(\boldsymbol{\alpha}_q^{\mathrm{c}}, t\right)/\partial\alpha_n\right|\Delta\alpha_{n,j_n}, \tag{13}$$

$$\overline{D}_{u_\tau u_\tau}\left(\boldsymbol{\alpha}_q^{\mathrm{I}}, t\right) = D_{u_\tau u_\tau}\left(\boldsymbol{\alpha}_q^{\mathrm{c}}, t\right) + \sum_{n=1}^{N}\left|\partial D_{u_\tau u_\tau}\left(\boldsymbol{\alpha}_q^{\mathrm{c}}, t\right)/\partial\alpha_n\right|\Delta\alpha_{n,j_n}, \tag{14}$$

where

$$D_{u_\tau u_\tau}\left(\boldsymbol{\alpha}_q^{\mathrm{c}}, t\right) = 2\Delta\omega\sum_{g=1}^{G} u_\tau\left(\boldsymbol{\alpha}_q^{\mathrm{c}}, \omega_g, t\right)\left\{u_\tau\left(\boldsymbol{\alpha}_q^{\mathrm{c}}, \omega_g, t\right)\right\}^*, \tag{15}$$

$$\partial D_{u_\tau u_\tau}\left(\boldsymbol{\alpha}_q^{\mathrm{c}}, t\right)/\partial\boldsymbol{\alpha}_n = 4\Delta\omega\sum_{g=1}^{G}\left\{\partial u_\tau\left(\boldsymbol{\alpha}_q^{\mathrm{c}}, \omega_g, t\right)/\partial\alpha_n\right\}\left\{u_\tau\left(\boldsymbol{\alpha}_q^{\mathrm{c}}, \omega_g, t\right)\right\}^*, \tag{16}$$

and |•| denotes the absolute value operator. In the interval perturbation analysis, the value of $\partial D_{u_\tau u_\tau}\left(\boldsymbol{\alpha}_q^{\mathrm{c}}, t\right)/\partial\alpha_n$ can also be called the sensitivity index, which is used to indicate the importance of the uncertainty input. In a well-known notation, the computational accuracy of the first-order expansion of an interval perturbation based on the Taylor series mainly relies on a slight fluctuation of uncertain parameters. However, the uncertainty level in practical engineering is always considerable due to the incomplete and imprecise uncertain information and knowledge constraint. Consequently, the uncertainty propagation results based on interval perturbation may be unacceptable for engineering applications. To improve the accuracy of the first-order perturbation, an adaptive sub-interval strategy is presented.

3.2. Sub-interval perturbation method

As discussed in the previous subsection, the accuracy of the first-order-based Taylor expansion suffers from high-level uncertainty. To overcome this deficiency, the sub-interval perturbation method is presented in this section. The component $\alpha_{n,j_n}^{\mathrm{I}}$ of the joint focal element α_q^{I} is considered to formulate the sub-interval strategy. When the number of sub-intervals of each component is R_n, then the r_nth sub-interval $(\alpha_{n,j_n}^{\mathrm{I}})_r$ of $\alpha_{n,j_n}^{\mathrm{I}}$ can be expressed as [34,35,37,38]

$$\left(\alpha_{n,j_n}^{\mathrm{I}}\right)_{r_n} = \left[\underline{\alpha}_{n,j_n} + 2\left(r_n - 1\right)\Delta\alpha_{n,j_n}/R_n, \underline{\alpha}_{n,j_n} + 2r_n\Delta\alpha_{n,j_n}/R_n\right]$$
$$r_n \in \forall[1, R_n] \quad j_n \in \forall[1, J_n] \quad n \in \forall[1, N]. \tag{17}$$

Thus, the joint sub-interval $\left(\boldsymbol{\alpha}_q^{\mathrm{I}}\right)_l$ of the joint focal element α_q^{I} is determined by:

$$\left(\boldsymbol{\alpha}_q^{\mathrm{I}}\right)_l = \left\{\left(\alpha_{1,j_1}^{\mathrm{I}}\right)_{r_1}, \ldots, \left(\alpha_{n,j_n}^{\mathrm{I}}\right)_{r_n}, \ldots, \left(\alpha_{n,j_N}^{\mathrm{I}}\right)_{r_N}\right\}$$
$$q \in \forall[1, \prod_{n=1}^{N} J_n], l \in \forall[1, \prod_{n=1}^{N} R_n]. \tag{18}$$

When two adjacent sub-intervals $\left(\boldsymbol{\alpha}_q^{\mathrm{I}}\right)_l = \left[\left(\alpha_{1,j_1}^{\mathrm{I}}\right)_{r_1}, \ldots, \left(\alpha_{n,j_n}^{\mathrm{I}}\right)_{r_n}, \ldots, \left(\alpha_{N,j_N}^{\mathrm{I}}\right)_{r_N}\right]^{\mathrm{T}}$ and $\left(\boldsymbol{\alpha}_q^{\mathrm{I}}\right)_{l+1} = \left[\left(\alpha_{1,j_1}^{\mathrm{I}}\right)_{r_1}, \ldots, \left(\alpha_{n,j_n}^{\mathrm{I}}\right)_{r_n+1}, \ldots, \left(\alpha_{N,j_N}^{\mathrm{I}}\right)_{r_N}\right]^{\mathrm{T}}$ of the joint focal element $\boldsymbol{\alpha}_q^{\mathrm{I}}$ are given, the following holds:

$$u_\tau\left(\left(\boldsymbol{\alpha}_q^{\mathrm{I}}\right)_l, \omega_g, t\right) \cap u_\tau\left(\left(\boldsymbol{\alpha}_q^{\mathrm{I}}\right)_{l+1}, \omega_g, t\right) = u_\tau\left(\left(\boldsymbol{\alpha}_q^{\mathrm{I}}\right)_l \cap \left(\boldsymbol{\alpha}_q^{\mathrm{I}}\right)_{l+1}, \omega_g, t\right), \tag{19}$$

in which,

$$\left(\boldsymbol{\alpha}_q^{\mathrm{I}}\right)_l \cap \left(\boldsymbol{\alpha}_q^{\mathrm{I}}\right)_{l+1} = \left[\left(\alpha_{1,j_1}^{\mathrm{I}}\right)_{r_1}, \ldots, \left(\bar{\alpha}_{n,j_n}\right)_{r_n}\right.$$
$$\left. = \left(\underline{\alpha}_{n,j_n}\right)_{r_n+1}, \ldots, \left(\alpha_{N,j_N}^{\mathrm{I}}\right)_{r_N}\right]^{\mathrm{T}}. \tag{20}$$

Then, using Eq. (19), the following conclusion for $D_{u_\tau u_\tau}\left(\boldsymbol{\alpha}_q^{\mathrm{I}}, t\right)$ is obtained:

$$D_{u_\tau u_\tau}\left(\left(\boldsymbol{\alpha}_q^{\mathrm{I}}\right)_l, t\right) \cap D_{u_\tau u_\tau}\left(\left(\boldsymbol{\alpha}_q^{\mathrm{I}}\right)_{l+1}, t\right) \neq \varnothing, \tag{21}$$

$$D_{u_\tau u_\tau}\left(\boldsymbol{\alpha}_q^{\mathrm{I}}, t\right) = \bigcup_{l\in[1, L_q]} D_{u_\tau u_\tau}\left(\left(\boldsymbol{\alpha}_q^{\mathrm{I}}\right)_l, t\right)$$
$$= \left[\min_{l\in[1, L_q]} \underline{D}_{u_\tau u_\tau}\left(\left(\boldsymbol{\alpha}_q^{\mathrm{I}}\right)_l, t\right), \max_{l\in[1, L_q]} \overline{D}_{u_\tau u_\tau}\left(\left(\boldsymbol{\alpha}_q^{\mathrm{I}}\right)_l, t\right)\right]. \tag{22}$$

where, $L_q = \prod_{n=1}^{N} R_n$ is the number of sub-intervals in joint focal element $\boldsymbol{\alpha}_q^{\mathrm{I}}$. From the aforementioned formulas, the accuracy of the sub-interval

perturbation strategy is guaranteed by the sufficiently small uncertain level of the sub-intervals of each uncertain parameter determined by the reasonable number R_n. However, computational efficiency sharply decreases with an increase in the number of sub-intervals. Therefore, a sensible strategy that involves balance between computational precision and consumption should be proposed.

3.3. Adaptive dimension reduction and subinterval updating strategy

As defined in Eq. (16), the $\partial D_{u_\tau u_\tau}\left(\boldsymbol{\alpha}_q^{\mathrm{c}}, t\right)/\partial\alpha_n$ is the sensitivity index of uncertain variable $\boldsymbol{\alpha}_n$ in joint focal element α_q^{I}. For concise, we use $A_q\left(\alpha_n, t\right)$ to denote the $\partial D_{u_\tau u_\tau}\left(\boldsymbol{\alpha}_q^{\mathrm{c}}, t\right)/\partial\alpha_n$. The reduction of the system input dimension is a sensible choice to alleviate the computational burden of uncertainty propagation. The sensitivity index $A_q(a_n, t)$ is multiplied by m_q of $\boldsymbol{\alpha}_q^{\mathrm{I}}$; hence, the new sensitivity index is defined as

$$A\left(\alpha_n, t\right) = \sum_{q=1}^{Q}\left|A_q\left(\alpha_n, t\right)\right| \times m_q \tag{23}$$

where, $Q = \prod_{n=1}^{N} J_n$. The nominal sensitivity is defined as Eq. (24) to represent the relative importance of each uncertain parameter in the entire time history.

$$\widetilde{A}(\alpha_n) = \int_0^{\mathrm{T}} A\left(\alpha_n, \tau\right) \times \alpha_n^0 \mathrm{d}\tau \Big/ \sum_{n=1}^{N}\int_0^{\mathrm{T}} A\left(\boldsymbol{\alpha}_n, \tau\right) \times \boldsymbol{\alpha}_n^0 \mathrm{d}\tau \tag{24}$$

where α_n^0 is the nominal value of uncertain parameter α_n. Eq. (24) shows that the product of the $A(a_n, t)$ and α_n^0 is used to avoid the discrepancy of the physical dimension of each uncertain parameter. The relative contribution of each uncertain parameter is determined by estimating the sensitivity index. The higher the value of $\tilde{A}(\alpha_n)$, the more important the contribution of the uncertain parameter, which shall be divided into more sub-intervals in the uncertainty propagation process. However, a smaller value of $\tilde{A}\left(\alpha_n\right)$ demonstrates the slight influence of α_n on system output, which shall be neglected in the uncertainty propagation to save computational cost. The selection of sub-interval numbers is flexible and efficient according to the different values of $\tilde{A}(\alpha_n)$ for each variable. After the dimension reduction, the sub-interval updating is employed to estimate the lower and upper bounds of system response. The strategy of sub-interval updating is defined as double of current number. The convergence criterion of ASPM is presented in Section 5, because of involving evidential uncertainty measurement.

3.4. Numerical evaluation of ASPM

From the aforementioned description of ASPM, the values of $\underline{D}_{u_\tau u_\tau}\left(\boldsymbol{\alpha}_q^{\mathrm{I}}, t\right)$ and $\overline{D}_{u_\tau u_\tau}\left(\boldsymbol{\alpha}_q^{\mathrm{I}}, t\right)$ are approximated by $\underline{D}_{u_\tau u_\tau}\left((\boldsymbol{\alpha}_q^{\mathrm{I}})_{\mathrm{lower}}, t\right)$ and $\overline{D}_{u_\tau u_\tau}\left((\boldsymbol{\alpha}_q^{\mathrm{I}})_{\mathrm{upper}}, t\right)$, where $\left(\boldsymbol{\alpha}_q^{\mathrm{I}}\right)_{\mathrm{lower}}$ and $\left(\boldsymbol{\alpha}_q^{\mathrm{I}}\right)_{\mathrm{upper}}$ denote the judicious sub-interval combination of the lower and upper bounds in the joint focal element α_q^{I}. Therefore, Eqs. (13) and (14) can be transformed into

$$\begin{aligned}\underline{D}_{u_\tau u_\tau}\left(\boldsymbol{\alpha}_q^{\mathrm{I}}, t\right) &= D_{u_\tau u_\tau}\left(\left(\boldsymbol{\alpha}_q^{\mathrm{I}}\right)_{\mathrm{lower}}^{\mathrm{c}}, t\right)\\ &- \sum_{n=1}^{N}\left|\partial D_{u_\tau u_\tau}\left(\left(\boldsymbol{\alpha}_q^{\mathrm{I}}\right)_{\mathrm{lower}}^{\mathrm{c}}, t\right)/\partial\alpha_n\right| \Delta\alpha_{n,j_n}/R_n\end{aligned} \tag{25}$$

$$\begin{aligned}\overline{D}_{u_\tau u_\tau}\left(\boldsymbol{\alpha}_q^{\mathrm{I}}, t\right) &= D_{u_\tau u_\tau}\left(\left(\boldsymbol{\alpha}_q^{\mathrm{I}}\right)_{\mathrm{upper}}^{\mathrm{c}}, t\right)\\ &+ \sum_{n=1}^{N}\left|\partial D_{u_\tau u_\tau}\left(\left(\boldsymbol{\alpha}_q^{\mathrm{I}}\right)_{\mathrm{upper}}^{\mathrm{c}}, t\right)/\partial\alpha_n\right| \Delta\alpha_{n,j_n}/R_n\end{aligned} \tag{26}$$

To estimate the right side of Eqs. (25) and (26), Eq. (1) is rewritten as a state function as follows:

$$\dot{\mathbf{y}}(\boldsymbol{\alpha}, \omega, t) = \mathbf{H}(\boldsymbol{\alpha})\mathbf{y}(\boldsymbol{\alpha}, \omega, t) + \mathbf{F}(\omega, t) \tag{27}$$

where

$$\begin{aligned}\mathbf{y}(\boldsymbol{\alpha}, t) &= \begin{bmatrix}\mathbf{u}\left(\boldsymbol{\alpha}, \omega, t\right)\\ \dot{\mathbf{u}}\left(\boldsymbol{\alpha}, \omega, t\right)\end{bmatrix},\\ \mathbf{H}\left(\boldsymbol{\alpha}\right) &= \begin{bmatrix}0 & \mathbf{E}_m\\ -\mathbf{M}^{-1}\left(\boldsymbol{\alpha}\right)\mathbf{K}\left(\boldsymbol{\alpha}\right) & -\mathbf{M}^{-1}\left(\boldsymbol{\alpha}\right)\mathbf{C}\left(\boldsymbol{\alpha}\right)\end{bmatrix}\end{aligned} \tag{28}$$

where $\mathbf{E}_{\mathrm{m}}$ is the identity matrix, and Eq. (27) is the state function of the system with uncertain parameters $\boldsymbol{\alpha}$. In this study, the time variant power spectral density of non-stationary stochastic excitation $\mathbf{S}\left(\boldsymbol{\omega}\right)$ is represented as the product of modulation function $g\left(t\right)$ and filtered white noise $\mathbf{S}_{ff}\left(\boldsymbol{\omega}\right)$. Thus, the stochastic excitation $\mathbf{F}(\omega, t)$ is characterized as [3,5]:

$$\mathbf{F}\left(\omega, t\right) = \left[0 \quad \mathrm{vec}\left(\mathbf{E}_m\sqrt{S_{ff}\left(\omega\right)}g(t)\exp\left(i\omega t\right)\right)\right]^{\mathrm{T}} \tag{29}$$

where vec(•) is the vectorization of the matrix, $g\left(t\right)$ is the uniform modulated envelope function. Evidently, the values of $u_\tau\left(\left(\boldsymbol{\alpha}_q^{\mathrm{I}}\right)_{\mathrm{lower}}^{\mathrm{c}}, \omega_g, t\right)$ and $u_\tau\left(\left(\boldsymbol{\alpha}_q^{\mathrm{I}}\right)_{\mathrm{upper}}^{\mathrm{c}}, \omega_g, t\right)$ are obtained by taking and solving $\left(\boldsymbol{\alpha}_q^{\mathrm{I}}\right)_{\mathrm{lower}}^{\mathrm{c}}$ and $\left(\boldsymbol{\alpha}_q^{\mathrm{I}}\right)_{\mathrm{upper}}^{\mathrm{c}}$ into Eq. (27) and using the highly precise direct-line integration method [3]. Taking the $u_\tau\left(\left(\boldsymbol{\alpha}_q^{\mathrm{I}}\right)_{\mathrm{lower}}^{\mathrm{c}}, \omega_g, t\right)$ and $u_\tau\left(\left(\boldsymbol{\alpha}_q^{\mathrm{I}}\right)_{\mathrm{upper}}^{\mathrm{c}}, \omega_g, t\right)$ into Eq. (15), the values of $D_{u_\tau u_\tau}\left(\left(\boldsymbol{\alpha}_q^{\mathrm{I}}\right)_{\mathrm{lower}}^{\mathrm{c}}, t\right)$ and $D_{u_\tau u_\tau}\left(\left(\boldsymbol{\alpha}_q^{\mathrm{I}}\right)_{\mathrm{upper}}^{\mathrm{c}}, t\right)$ are obtained. Moreover, the values of $\partial u_\tau\left(\left(\boldsymbol{\alpha}_q^{\mathrm{I}}\right)_{\mathrm{lower}}^{\mathrm{c}}, \omega_g, t\right)/\partial\alpha_n$ and $\partial u_\tau\left(\left(\boldsymbol{\alpha}_q^{\mathrm{I}}\right)_{\mathrm{upper}}^{\mathrm{c}}, \omega_g, t\right)/\partial\alpha_n$ are evaluated by replacing $\boldsymbol{\alpha}$ with $\left(\boldsymbol{\alpha}_q^{\mathrm{I}}\right)_{\mathrm{lower}}^{\mathrm{c}}$ and $\left(\boldsymbol{\alpha}_q^{\mathrm{I}}\right)_{\mathrm{upper}}^{\mathrm{c}}$ in the following expression:

$$\frac{\partial\dot{\mathbf{y}}(\boldsymbol{\alpha}, \omega, t)}{\partial\boldsymbol{\alpha}_n} = \mathbf{H}(\boldsymbol{\alpha})\frac{\partial\mathbf{y}(\boldsymbol{\alpha}, \omega, t)}{\partial\boldsymbol{\alpha}_n} + \frac{\partial\mathbf{H}(\boldsymbol{\alpha})}{\partial\boldsymbol{\alpha}_n}\mathbf{y}(\boldsymbol{\alpha}, \omega, t) + \frac{\partial\mathbf{F}\left(\omega, t\right)}{\partial\boldsymbol{\alpha}_n} \tag{30}$$

where

$$\frac{\partial\mathbf{y}\left(\boldsymbol{\alpha}, \omega, t\right)}{\partial\boldsymbol{\alpha}_n} = \begin{bmatrix}\dfrac{\partial\dot{\mathbf{u}}\left(\boldsymbol{\alpha}, \omega, t\right)}{\partial\boldsymbol{\alpha}_n}\\ \dfrac{\partial\mathbf{u}\left(\boldsymbol{\alpha}, \omega, t\right)}{\partial\boldsymbol{\alpha}_n}\end{bmatrix} \quad \frac{\partial\mathbf{H}\left(\boldsymbol{\alpha}\right)}{\partial\boldsymbol{\alpha}_n} = \begin{bmatrix}0 & 0\\ \dfrac{\partial\mathbf{H}_3\left(\boldsymbol{\alpha}\right)}{\partial\boldsymbol{\alpha}_n} & \dfrac{\partial\mathbf{H}_4\left(\boldsymbol{\alpha}\right)}{\partial\boldsymbol{\alpha}_n}\end{bmatrix} \tag{31}$$

$$\frac{\partial\mathbf{H}_3\left(\boldsymbol{\alpha}\right)}{\partial\boldsymbol{\alpha}_n} = -\frac{\partial\mathbf{M}^{-1}\left(\boldsymbol{\alpha}\right)}{\partial\boldsymbol{\alpha}_n}\mathbf{K}\left(\boldsymbol{\alpha}\right) - \mathbf{M}^{-1}\left(\boldsymbol{\alpha}\right)\frac{\partial\mathbf{K}\left(\boldsymbol{\alpha}\right)}{\partial\boldsymbol{\alpha}_n} \tag{32}$$

$$\frac{\partial\mathbf{H}_4\left(\boldsymbol{\alpha}\right)}{\partial\boldsymbol{\alpha}_n} = -\frac{\partial\mathbf{M}^{-1}\left(\boldsymbol{\alpha}\right)}{\partial\boldsymbol{\alpha}_n}\mathbf{C}\left(\boldsymbol{\alpha}\right) - \mathbf{M}^{-1}\left(\boldsymbol{\alpha}\right)\frac{\partial\mathbf{C}\left(\boldsymbol{\alpha}\right)}{\partial\boldsymbol{\alpha}_n} \tag{33}$$

The value of $\partial D_{u_\tau u_\tau}\left(\left(\boldsymbol{\alpha}_q^{\mathrm{I}}\right)_{\mathrm{lower}}^{\mathrm{c}}, t\right)/\partial\alpha_{\mathrm{n}}$ is calculated by substituting the obtained $\partial u_\tau\left(\left(\boldsymbol{\alpha}_q^{\mathrm{I}}\right)_{\mathrm{lower}}^{\mathrm{c}}, \omega_g, t\right)/\partial\boldsymbol{\alpha}_{\mathrm{n}}$ and $u_\tau\left(\left(\boldsymbol{\alpha}_q^{\mathrm{I}}\right)_{\mathrm{lower}}^{\mathrm{c}}, \omega_g, t\right)$ into Eq. (16). The value of $\partial D_{u_\tau u_\tau}\left(\left(\boldsymbol{\alpha}_q^{\mathrm{I}}\right)_{\mathrm{upper}}^{\mathrm{c}}, t\right)/\partial\alpha_{\mathrm{n}}$ is given using the same operation. Then, the lower and upper bounds of $D_{u_\tau u_\tau}\left(\boldsymbol{\alpha}_q^{\mathrm{I}}, t\right)$ are obtained using Eqs. (25) and (26).

4. Uncertainty measurement for the transient response of a dynamic system

After the uncertainty propagation step, the lower and upper response bounds of the system response for each joint focal element $\boldsymbol{\alpha}_q^{\mathrm{I}}$ are obtained. Evidence theory uses the belief (*Bel*) and plausibility (*Pl*) measures to characterize uncertainty by indicating the confident degree to determine whether an event is true or false. Similar to the previous sections, we set sample $x \in \Omega$ and $A_k = \left[\underline{a}_k, \bar{a}_k\right]\ k \in \forall[1, K]$ is the proposition in power set Θ, and m_k is the BBA of proposition A_k. Given subset $L_x = \left\{x | x \in \Omega, -\infty \le x \le x_{\mathrm{thre}}\right\}$, $Bel\left(L_x\right)$ and $Pl\left(L_x\right)$ can be built using the belief cumulative distribution function (BCDF) proposed by Yager [40] and Durante [41]:

$$Bel\left(L_x\right) = \sum_{\bar{a}_k \le x_{\mathrm{thre}}} m_k \tag{34}$$

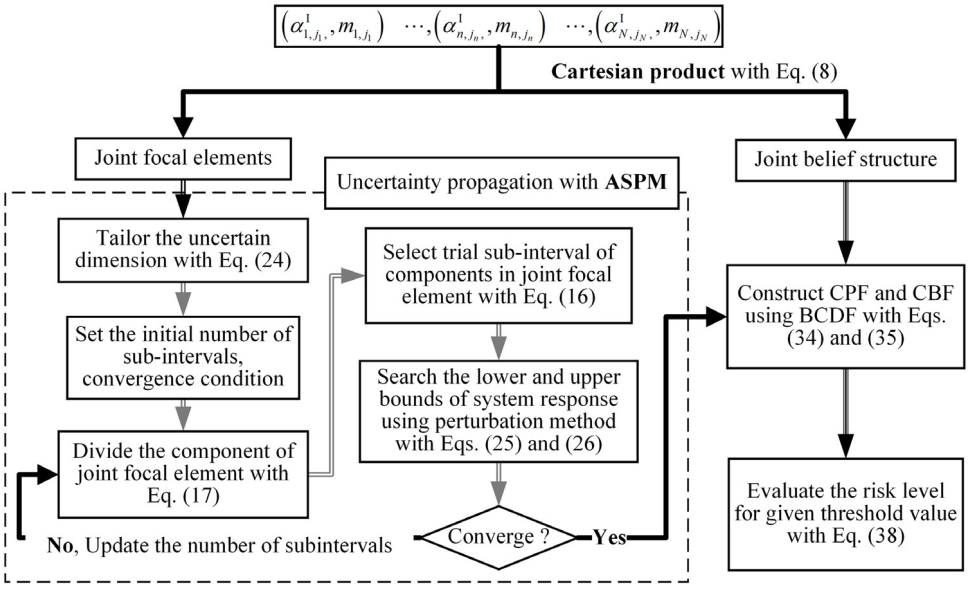

Fig. 1. Flowchart of evidential UQ using ASPM.

$$Pl\left(L_x\right) = \sum_{\underline{a}_k \le x_{\text{thre}}} m_k \tag{35}$$

in which, $Bel\ (L_x)$ and $Pl\ (L_x)$ are also called the cumulative belief function (CBF) and the cumulative plausibility function (CPF). Then, the complete expression for the BCDF of x_{thre} holds:

$$F_m\left(x_{\text{thre}}\right) = \left[Bel\left(L_x\right), Pl(L_x)\right] \tag{36}$$

Given a designated BCDF, $F_m\left(x_{\text{thre}}\right) = [Bel\left(L_x\right), Pl(L_x)]$, the lower and upper bounds of x_{thre}, corresponding to a threshold exceedance probability p_{thre} is obtained as:

$$\left[\underline{x}_{\text{thre}}, \bar{x}_{\text{thre}}\right] = \left[Pl^{-1}(p_{\text{thre}}), Bel^{-1}(p_{\text{thre}})\right] \tag{37}$$

In stochastic dynamic analysis, given the propagated focal elements and associated belief structure of the variance response of interesting displacement $\left(\left[\left(\underline{D}_{u_\tau u_\tau}\right)_1, \left(\overline{D}_{u_\tau u_\tau}\right)_1\right], m_1\right), \ldots, \left(\left[\left(\underline{D}_{u_\tau u_\tau}\right)_q, \left(\overline{D}_{u_\tau u_\tau}\right)_q\right], m_q\right), \cdots, \left(\left[\left(\underline{D}_{u_\tau u_\tau}\right)_Q, \left(\overline{D}_{u_\tau u_\tau}\right)_Q\right], m_Q\right)$ the lower and upper bounds of $\left(D_{u_\tau u_\tau}\right)_{\text{thre}}$ for p_{thre} can be constructed using the following expression:

$$\left[\left(\underline{D}_{u_\tau u_\tau}\right)^{p_{\text{thre}}}, \left(\overline{D}_{u_\tau u_\tau}\right)^{p_{\text{thre}}}\right] = \left[Pl^{-1}(p_{\text{thre}}), Bel^{-1}(p_{\text{thre}})\right] \tag{38}$$

Evidently, the distances of $\left(\underline{D}_{u_\tau u_\tau}\right)^{p_{\text{thre}}}$ and $\left(\overline{D}_{u_\tau u_\tau}\right)^{p_{\text{thre}}}$ in Eq. (38) represent the knowledge and completeness levels of the uncertain information for structural parameter $\boldsymbol{\alpha}$. The tight ranges of $\left(\underline{D}_{u_\tau u_\tau}\right)^{p_{\text{thre}}}$ and $\left(\overline{D}_{u_\tau u_\tau}\right)^{p_{\text{thre}}}$ suggest the complete uncertain information and perfect knowledge of $\boldsymbol{\alpha}$ with minimal epistemic and vice versa.

5. Summary of evidential UQ with ASPM

To sum up above mentioned sections, the uncertainty propagation using ASPM is addressed in the evidential UQ framework. The adaptive scheme for sub-interval perturbation consists of three stages: the dimensional reduction using the global sensitivity analysis, sub-interval updating and convergence estimation. The convergence criterion is constructed by using the maximum of relative error of $\left(\underline{D}_{u_\tau u_\tau}\right)^{0.5}$ and $\left(\overline{D}_{u_\tau u_\tau}\right)^{0.5}$ corresponding to the former and latter iterations. To illustrate the evidential UQ with ASPM more detail, the flowchart are summarized as in Fig. 1.

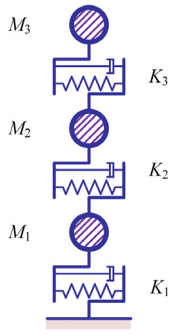

Fig. 2. Three DOF system.

Table 1
Focal elements and belief structure of variables.

K (kN/m)		M (kg)	
Focal element	BBA	Focal element	BBA
[13 600, 16 000]	0.2	[8000, 9500]	0.15
[15 200, 16 800]	0.6	[9000, 10 000]	0.35
[16 000, 18 400]	0.2	[10 000, 11 000]	0.35
		[10 500, 12 000]	0.15

6. Case study

6.1. Three degree-of-freedom (DOF) system

The three DOF system (Fig. 2) is excited by white noise with PSD intensity $S_0 = 0.001574\ \text{m}^2/\text{s}^3$. All the nodes have the same nominal mass $M_i = 10^4$ kg and nominal stiffness $K_i = 16\,000\text{kN/m}\ (i = 1, 2, 3)$. The damping ratio for all the modes is assumed $\xi = 0.05$. The variance of the horizontal displacement of the third node $D_{u_3u_3}(t)$ is considered response quantities of interest. The uncertain information of stiffness K and lumped mass of nodes M is presented in Table 1.

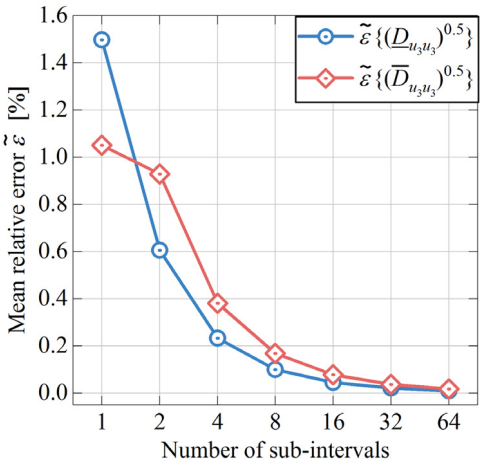

Fig. 4. Variation of the mean relative error with an increment in the number of sub-intervals.

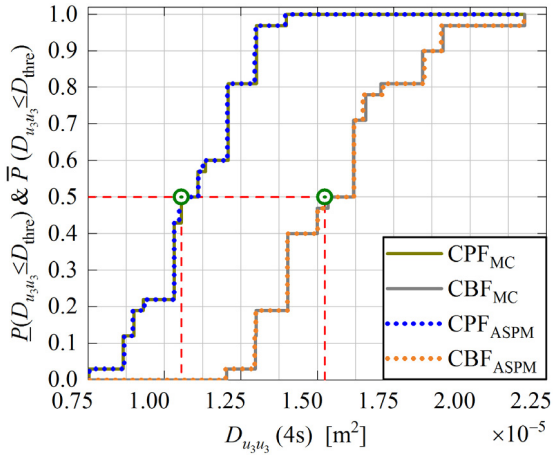

Fig. 5. Comparison of the cumulative distribution of $D_{u_3u_3}(4\text{ s})$ obtained using ASPM and MC simulation with 10^5 samples.

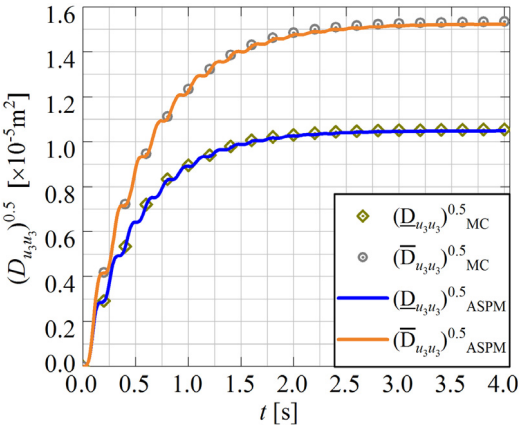

Fig. 6. Comparison of the upper and lower bounds of $(D_{u_3u_3})^{0.5}$ in the time history obtained using ASPM and MC simulation with 10^5 samples.

Using the information provided in Table 1, the joint uncertain input $\boldsymbol{\alpha}_q^{\text{I}}$ is consolidated by the Cartesian product as follows:

$$\boldsymbol{\alpha}_q^{\text{I}} = [K_{j_1}^{\text{I}}, M_{j_2}^{\text{I}}]^{\text{T}} \quad m_q = m_{j_1} \times m_{j_2}$$
$$j_1 \in \forall[1,3] \quad j_2 \in \forall[1,4] \quad q \in \forall[1,12], \tag{39}$$

where $\sum_{q=1}^{12} m_q = 1$. When the joint focal element of design variable $\boldsymbol{\alpha}_q^{\text{I}}$ is substituted into the framework of evidential UQ, the gradient of each variable for joint focal element $A_q(\alpha_n, t)$ is obtained using Eq. (15). The gray lines shown in Fig. 3(a)–(b), in which (a) stiffness K and (b) lumped node mass M, are the gradients of the $D_{u_3u_3}(t)$ of each joint focal element for uncertain parameters. The red lines in Fig. 3(a)–(b) denote the evidential sensitivity index $A(\alpha_n, t)$ computed by Eq. (23).

As shown in Fig. 3(a), the gradient value of stiffness K is negative, which indicates that an increment of stiffness K produces a negative decrement of $D_{u_3u_3}(t)$ in the time history. Meanwhile, Fig. 3(b) illustrates that lumped mass M produces a positive impact on $D_{u_3u_3}(t)$ in the time history. When Eq. (24) is used, the values of $\tilde{A}(K)$ and $\tilde{A}(M)$ are calculated as 0.5 and 0.5, respectively, thereby indicating that the contributions of stiffness and lumped mass are important. In accordance with the aforementioned sensitivity analysis results, the focal elements of K and M shall be decomposed into sub-intervals. The initial value of a sub-interval is set as $R_n = 1$, and the threshold value of convergence factor $\varepsilon_{\text{thre}}$ is 1%. The relative error values of the lower and upper bounds of expectation $\left\{D_{u_3u_3}(t)\right\}^{0.5}$ in the time history are used to denote the convergence condition.

$$\tilde{\varepsilon}\left\{\left(\underline{D}_{u_3u_3}\right)^{0.5}\right\} = \left|\left(\underline{D}_{u_3u_3}\right)^{0.5}_{2R_n} - \left(\underline{D}_{u_3u_3}\right)^{0.5}_{R_n}\right| \Big/ \left(\underline{D}_{u_3u_3}\right)^{0.5}_{2R_n} \times 100\%, \tag{40}$$

$$\tilde{\varepsilon}\left\{\left(\overline{D}_{u_3u_3}\right)^{0.5}\right\} = \left|\left(\overline{D}_{u_3u_3}\right)^{0.5}_{2R_n} - \left(\overline{D}_{u_3u_3}\right)^{0.5}_{R_n}\right| \Big/ \left(\overline{D}_{u_3u_3}\right)_{2R_n} \times 100\%, \tag{41}$$

$$\max\left[\tilde{\varepsilon}\left\{\left(\underline{D}_{u_3u_3}\right)^{0.5}\right\}, \tilde{\varepsilon}\left\{\left(\overline{D}_{u_3u_3}\right)^{0.5}\right\}\right] \le \varepsilon_{\text{thre}}, \tag{42}$$

where $\left(D_{u_3u_3}\right)^{0.5}_{R_n}$ and $\left(D_{u_3u_3}\right)^{0.5}_{2R_n}$ are the UQ results of the component of joint focal element $\boldsymbol{\alpha}_q^{\text{I}}$, which is divided into R_n and $2R_n$ sub-intervals. The variations of $\tilde{\varepsilon}$ with the increased number of sub-intervals are shown in Fig. 4.

As shown in Fig. 4, convergence factor $\tilde{\varepsilon}$ gradually approximates threshold value $\varepsilon_{\text{thre}}$ along with an increment in the number of sub-intervals. $\tilde{\varepsilon}\left\{\left(\underline{D}_{u_3u_3}\right)^{0.5}\right\}$ and $\tilde{\varepsilon}\left\{\left(\overline{D}_{u_3u_3}\right)^{0.5}\right\}$ are smaller than threshold value $\varepsilon_{\text{thre}}$ when the number of sub-intervals increases to four. That is, the propagation results obtained using ASPM with four sub-intervals can be adopted to represent the UQ results of this problem.

To test the precision of the proposed ASPM, the result obtained via MC simulation is used as the reference. The MC simulation with 10^5 samples are implemented to search for the maximum and minimum system responses that correspond to each joint focal element $\boldsymbol{\alpha}_q^{\text{I}}$. After the propagation of uncertainties, the CPF and CBF for different threshold values are constructed by using Eqs. (34) and (35). Fig. 5 shows the evidential UQ results obtained via ASPM with four sub-intervals and the results computed via MC simulation at 4 s. To present the quantitative comparison of the accuracy of ASPM, Table 2 summarizes the lower and upper bounds and the relative error of the expectation of $D_{u_3u_3}(t)$ with 0.5 exceedance probabilities for four sub-intervals at 4 s. The comparison of the presented ASPM and the reference of the $D_{u_3u_3}(t)$ with 0.5 exceedance probabilities in the entire time history is shown in Fig. 6.

As shown in Fig. 5, the CPF and CBF curves of $D_{u_3u_3}(4\text{ s})$ obtained via ASPM with four sub-intervals match well with the results obtained via MC with 10^5 sample numbers, thereby indicating that the proposed ASPM provides high precision for estimating $D_{u_3u_3}(4\text{ s})$. The same scenario is reflected in Fig. 6, in which the proposed ASPM yields an accurate approximation of the time history curves of the lower and upper bounds of $D_{u_3u_3}(t)$, which is calculated via MC simulation with 10^5 samples. In accordance with the situation reflected in Table 2, the maximum errors for the lower and upper bounds of $\left(D_{u_3u_3}\right)^{0.5}$ are 0.663% and 0.717%, respectively. This finding demonstrates that the

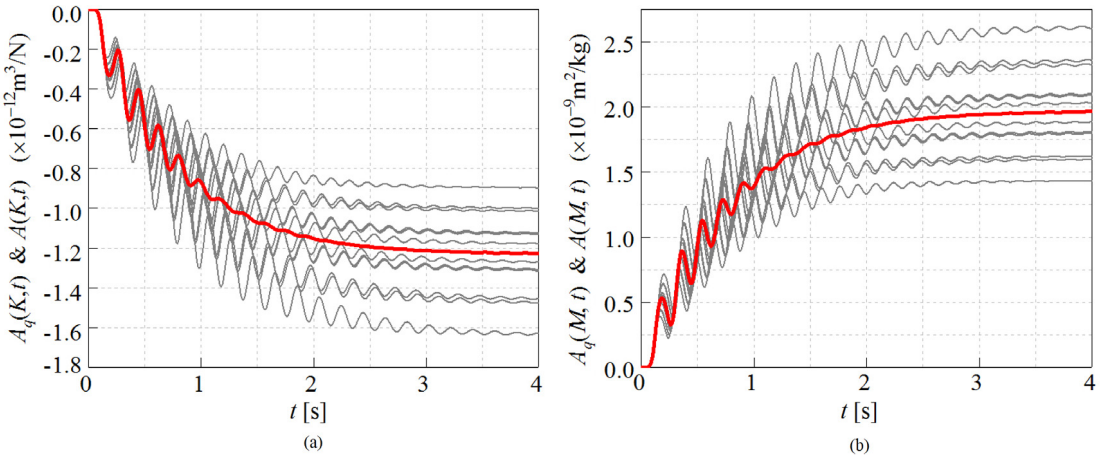

Fig. 3. First-order sensitivities of $D_{u_3u_3}(t)$ with respect to the parameters: (a) stiffness K and (b) lumped mass M.

Table 2
Comparison of the lower and upper bounds of $\left(D_{u_3u_3}\right)^{0.5}$ obtained using ASPM and MC with 10^5 samples.

T (s)		ASPM ($\times 10^{-5}$ m^2)	MC ($\times 10^{-5}$ m^2)	Relative errors (%)
4.0	Lower bound	1.048	**1.055**	**0.663**
	Upper bound	1.524	**1.535**	**0.717**

proposed ASPM exhibits high precision in searching for the boundary system response of the joint focal element.

6.2. Plane truss

As shown in Fig. 7, two bay plane trusses with 27 bars and 18 nodes are presented to investigate the performance of the ASPM-based evidential UQ method. The Young's modulus, cross section, and material density of the truss elements, and the lumped node mass are assumed as uncertain variables. The nominal values of the Young's modulus $E_0 = 2.1 \times 10^{11}$ N/m^2, cross section $A_0 = 5 \times 10^{-4}$ m^2, material density $\rho_0 = 7800$ kg/m^3, and lumped mass $M_0 = 500$ kg are assumed in the UQ process. The focal element sets and the corresponding belief structures of uncertain variables are collocated in Table 3. Rayleigh damping $\mathbf{C}(\boldsymbol{\alpha}) = c_0\mathbf{M}(\boldsymbol{\alpha}) + c_1\mathbf{K}(\boldsymbol{\alpha})$ is assumed to denote the damping matrix, and the damping ratios c_0 and c_1 are given by assuming the mode damping ratio $\xi = 0.05$ for the first and second modes. In this study, the Kanai–Tajimi model designated in [32] is used to denote the stochastic input $S_{ff}(\omega)$ of the system:

$$S_{ff}(\omega) = S_0 \frac{4\varsigma_g^2\omega_g^2\omega^2 + \omega_g^4}{\left(\omega_g^2 - \omega^2\right)^2 + 4\varsigma_g^2\omega_g^2\omega^2}, \tag{43}$$

where the constant PSD intensity of the bed rock $S_0 = 0.05$ m^2/s^3, the efficient damping ratio of the ground $\xi_g = 0.6$, and ground frequency $\omega_g = 4\pi$ rad/s. To reflect the intensity variation based on time, the following uniform modulate function is used:

$$g(t) = \boldsymbol{\alpha}\left(e^{-\beta_1 t} - e^{-\beta_2 t}\right), \tag{44}$$

where $\beta_1 = 2.5$ and $\beta_2 = 2.7$ are the attenuation ratios of the stationary section, and $\boldsymbol{\alpha} = 35.33$ is the intensity ratio. In this study, the variance of the horizontal displacement response of node 10 in time history $D_{u_{10}u_{10}}(t)$ is considered the response quantity of interest.

Using the uncertain information given in Table 3, the joint focal elements and corresponding belief structures of uncertain design vectors can be constructed using the Cartesian product.

$$\boldsymbol{\alpha}_q^{\mathrm{I}} = [E_{j_1}^{\mathrm{I}}, A_{j_2}^{\mathrm{I}}, \rho_{j_3}^{\mathrm{I}}, M_{j_4}^{\mathrm{I}}] \quad m_q = \prod_{n=1}^{4} m_{j_n}$$
$$j_1 \in \forall[1,4] \quad j_2 \in \forall[1,2] \quad j_3 \in \forall[1,2] \quad j_4 \in \forall[1,3] \tag{45}$$

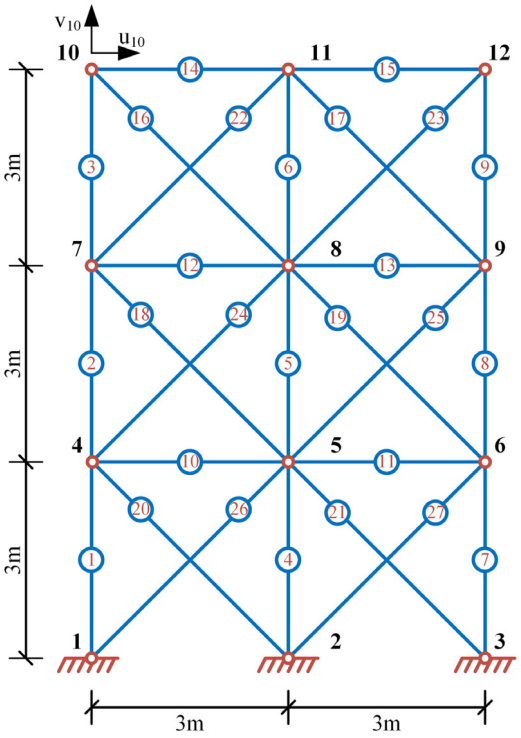

Fig. 7. Layout of the 27 bar trusses.

where $\sum_{q=1}^{36} m_q = 1$. When the joint focal element of design variable $\boldsymbol{\alpha}_q$ is substituted into the framework of evidential UQ, the gradient of each variable for joint focal element $A_q(\boldsymbol{\alpha}_n, t)$ are obtained using Eq. (16). The gray lines shown in Fig. 8(a)–(d) are the gradients of the $D_{u_{10}u_{10}}(t)$ of each joint focal element for uncertain parameters, such as (a) Young's modulus E, (b) truss element cross section A, (c) truss element material density ρ, and (d) lumped node mass M. The red lines in Fig. 8(a)–(d) denote the evidential sensitivity index $A(\boldsymbol{\alpha}_n, t)$ of the four aforementioned variables.

Table 3
Focal elements and belief structures of the variables.

E ($\times 10^{11}$ N/m^2)		A ($\times 10^{-4}$ m^2)		ρ (kg/m^3)		M (kg)	
Focal element	BBA	Focal element	BBA	Focal element	BBA	Focal element	BBA
[1.785, 2.1]	0.2	[4.5, 5.0]	0.5	[7020, 8190]	0.5	[400, 450]	0.15
[1.89, 2.205]	0.6	[5.0, 5.5]	0.5	[7800, 8580]	0.5	[450, 550]	0.7
[2.205, 2.415]	0.2					[550, 600]	0.15

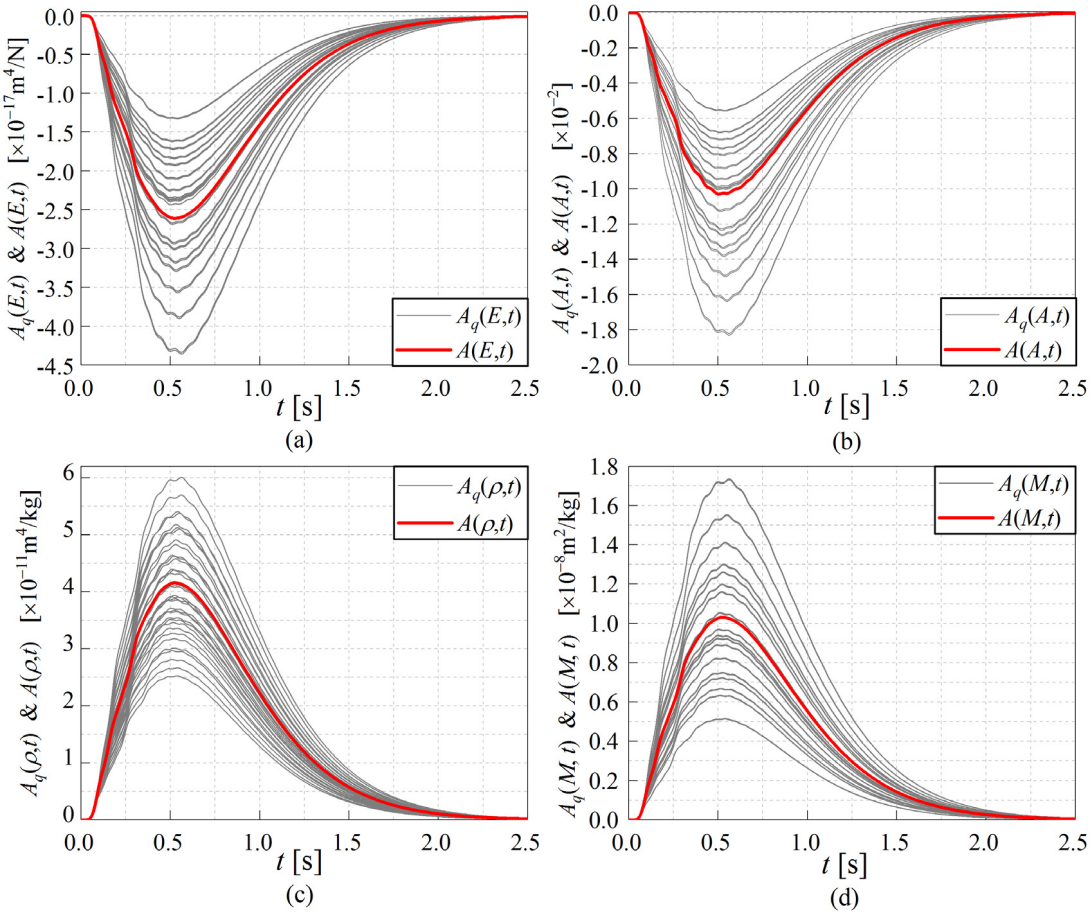

Fig. 8. First-order sensitivities of $D_{u_{10}u_{10}}$ to the parameters: (a) Young's modulus E, (b) truss element cross section A, (c) truss element material density ρ, and (d) lumped node mass M. (For interpretation of the references to color in this figure legend, the reader is referred to the web version of this article.)

As shown in Fig. 8(a) and (b), the gradient values of Young's modulus E and cross section A are negative, thereby indicating that an increment in Young's modulus E and cross section A produces a negative decrement of $D_{u_{10}u_{10}}(t)$ in the time history. Evidently, Fig. 8(c) and (d) demonstrate that the material density of truss elements ρ and the lumped mass of nodes M exert a positive impact on $D_{u_{10}u_{10}}(t)$ in the time evolution history. To utilize the feasibility for reducing computational cost, the nominal sensitivity index of the time history is calculated using Eq. (24). The bars in Fig. 9 indicate the nominal sensitivity indices of variables E, A, ρ, and M.

The nominal values of the four aforementioned variables presented in Fig. 9 for the nominal sensitivity values of variables E, A, ρ, and M are 0.3333, 0.3333, 0.0195, and 0.3138, respectively. The influence of variable ρ can be disregarded compared with the contributions of variables E, A, and M based on the critical information indicated in Fig. 9. The information presented in this figure provides the evidence to tailor the unimportant variable in the UQ process. In consideration of this scenario, the focal elements of variable ρ shall remain intact whereas the focal elements of the other components in vector $\boldsymbol{\alpha}_q^I$ shall be divided into several sub-intervals.

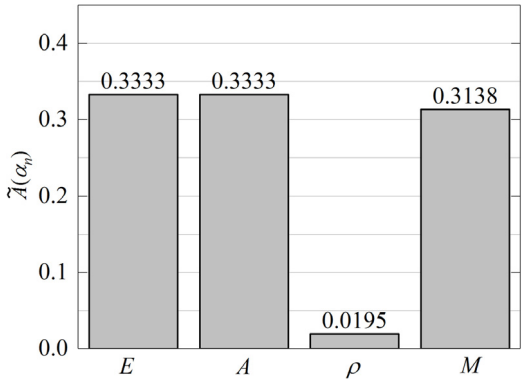

Fig. 9. Nominal sensitivity indices of the time history for variables E, A, ρ, and M.

Prior to uncertainty propagation, the initial value of the sub-interval and the threshold value of the convergence condition are set to same values as those in Case 1. In this case, the mean values of the relative

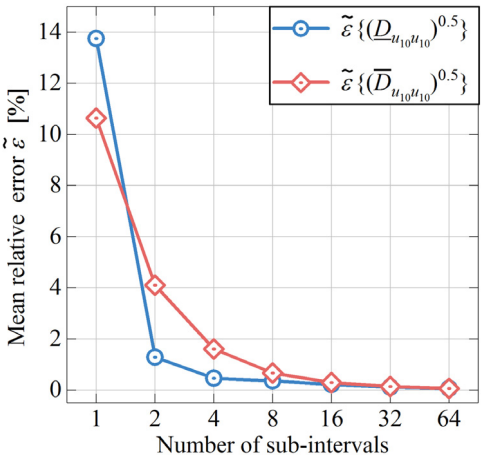

Fig. 10. Variation of the mean relative error with an increment in the number of sub-intervals.

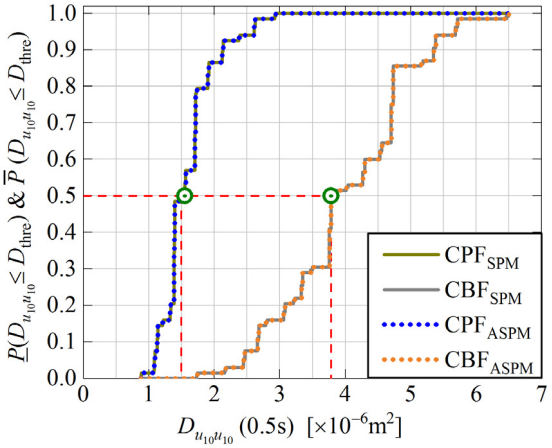

Fig. 11. Comparison of the cumulative distribution of $D_{u_{10}u_{10}}(t)$ provided by ASPM and SPM at 0.5 s.

error of the lower and upper bounds of expectation in the time history $\tilde{\varepsilon}\left\{\left(\underline{D}_{u_{10}u_{10}}\right)^{0.5}\right\}$ and $\tilde{\varepsilon}\left\{\left(\overline{D}_{u_{10}u_{10}}\right)^{0.5}\right\}$ are used to denote the convergence condition. The variations of ε with an increment in the number of sub-intervals are shown in Fig. 10.

As shown in Fig. 10, the convergence factor $\tilde{\varepsilon}$ gradually approximates the threshold value $\varepsilon_{\text{thre}}$ along with the increment in the number of sub-intervals. The values of ε of the lower and upper bounds of $\left(D_{u_{10}u_{10}}\right)^{0.5}$ are smaller than the threshold value $\varepsilon_{\text{thre}}$ when the number of sub-intervals increases to 8. That is, the propagation result obtained via ASPM with eight sub-intervals can be used to solve the result in the evidential UQ of $D_{u_{10}u_{10}}(t)$. To test the feasibility and efficiency of the tailored strategy, the classical SPM analysis for evidential propagation is presented. In SPM, the four components of focal element $\boldsymbol{\alpha}_q$ are divided into eight sub-intervals. The BCDF is implemented to construct the CPF and CBF of designated threshold values. Fig. 11 presents the comparison of the CPF and CBF curves of $D_{u_{10}u_{10}}(t)$ in the 0.5 s time cut provided by ASPM and SPM.

Fig. 11 depicts that the CPF and CBF curves of $D_{u_{10}u_{10}}(t)$ at 0.5 s provided by ASPM coincide with the results obtained by SPM. This finding indicates that the computational accuracies of ASPM and SPM are nearly equivalent. In addition to the comparison at the designated time cut, Fig. 12 describes the computational accuracy of ASPM in the entire time history by comparing the time evolutions of the lower and upper bounds of $(D_{u_{10}u_{10}})^{0.5}$ computed by SPM. Meanwhile, Table 4

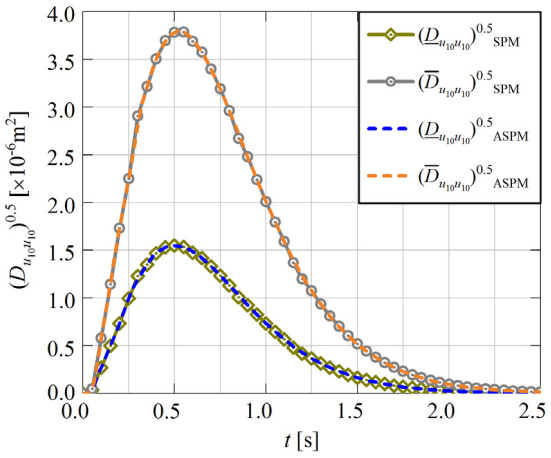

Fig. 12. Comparison of the upper and lower bounds of $(D_{u_{10}u_{10}})^{0.5}$ in the time history obtained via ASPM and SPM.

summarizes the comparison of the computational results obtained via ASPM and the classical SPM with eight sub-intervals, which correspond to the relative errors at 0.5, 1.25, 1.75 and 2.25 s.

As illustrated in Fig. 12, the lower and upper bounds of $\left(D_{u_{10}u_{10}}\right)^{0.5}_{\text{ASPM}}$ in the time history curves obtained via ASPM match well with the results obtained via SPM. That is, the accuracy of ASPM is always guaranteed. The same tendency is observed in Table 4, where the computational results computed via ASPM match well with the results obtained via SPM, and the relative error is limited and lower than 0.5%. Although the relative error is gradually increased with an increment in time history, the computational results are ignored compared with the maximum value in the time history. Critical information is also reflected in Figs. 11 and 12 and Table 4. The influence of component ρ on $D_{u_{10}u_{10}}$ is insignificant, and thus, can be neglected.

Evidence theory has always been used to deal with sparse and multi-source uncertainties. The distance between the CPF and CBF curves is used to denote the epistemic uncertainty of system response. BBA progressively approaches the continuous probability distribution with increasing uncertain information according to the intuitive observation of evidence theory [42–44]. That is, a decrease in epistemic uncertainty in system response is accompanied by the accumulation of the uncertain information of system input. However, the collection of uncertain information remains a challenging task because of the high cost and time consumption. The basic concept of sensitivity analysis suggests that the most important variable will produce the most essential changes in uncertain system response. To validate the effectiveness of the proposed sensitivity procedure, the completed evidential representations of variables E, A, ρ, and M are presented in Table 5.

The validation procedure consists of five analogous cases. In the first case, the evidential representation of Young's modulus is fixed as Table 3, whereas the uncertain information of cross section A, material density ρ, and lumped node mass M are signified by the evidential representations in Table 5. The propagation results CPF_1 and CPF_2 are shown in Fig. 13(a). The UQ results of CPF_2 and CBF_2 in Fig. 13(b) correspond to the evidential representation of the UQ results for the fixed variable cross section A, as shown in Table 3. However, the evidential representations of the other variables are updated, as shown in Table 5. The CPF_3, CBF_3, CPF_4, and CBF_4 as shown in Fig. 13(c) and (d) are obtained by fixing variables ρ and M, respectively. The CPF_5 and CBF_5 curves in Fig. 13 are obtained by updating the evidential representations of the four variables, as shown in Table 5. The evidential UQ results CPF_0 and CBF_0 in Fig. 13 are computed using the original uncertain information given in Table 3.

As shown in the four subfigures of Fig. 13, the distances of the CPF_5 and CBF_5 curves are significantly decreased compared with the

Table 4
Comparison of the lower and upper bounds of $\left(D_{u_{10}u_{10}}\right)^{0.5}$ obtained via ASPM and SPM at different time cuts.

T (s)	Lower bound			Upper bound		
	ASPM ($\times 10^{-6}$ m^2)	SPM ($\times 10^{-6}$ m^2)	Relative errors (%)	ASPM ($\times 10^{-6}$ m^2)	SPM ($\times 10^{-6}$ m^2)	Relative errors (%)
0.5	1.551	1.551	0.015	3.780	3.782	0.063
1.25	0.370	0.370	0.106	1.076	1.077	0.160
1.75	0.070	0.070	0.172	0.232	0.233	0.239
2.25	0.011	0.011	**0.234**	0.040	0.040	**0.327**

Table 5
Focal elements and belief structures of the variables.

E ($\times 10^{11}$ N/m^2)		A ($\times 10^{-4}$ m^2)		ρ (kg/m^3)		M (kg)	
Focal element	BBA	Focal element	BBA	Focal element	BBA	Focal element	BBA
[1.780, 1.943]	0.1	[4.500, 4.625]	0.1	[7020, 7332]	0.125	[400, 425]	0.075
[1.943, 2.100]	0.1	[4.625, 4.750]	0.1	[7332, 7605]	0.125	[425, 450]	0.075
[1.890, 1.995]	0.15	[4.750, 4.875]	0.15	[7605, 7800]	0.125	[450, 475]	0.175
[1.995, 2.100]	0.15	[4.875, 5.000]	0.15	[7800, 8190]	0.125	[475, 500]	0.175
[2.100, 2.153]	0.15	[5.000, 5.125]	0.15	[7410, 7722]	0.125	[500, 525]	0.175
[2.153, 2.205]	0.15	[5.125, 5.250]	0.15	[7722, 7995]	0.125	[525, 550]	0.175
[2.205, 2.310]	0.1	[5.250, 5.375]	0.1	[7995, 8268]	0.125	[550, 575]	0.075
[2.310, 2.415]	0.1	[5.375, 5.500]	0.1	[8268, 8580]	0.125	[575, 600]	0.075

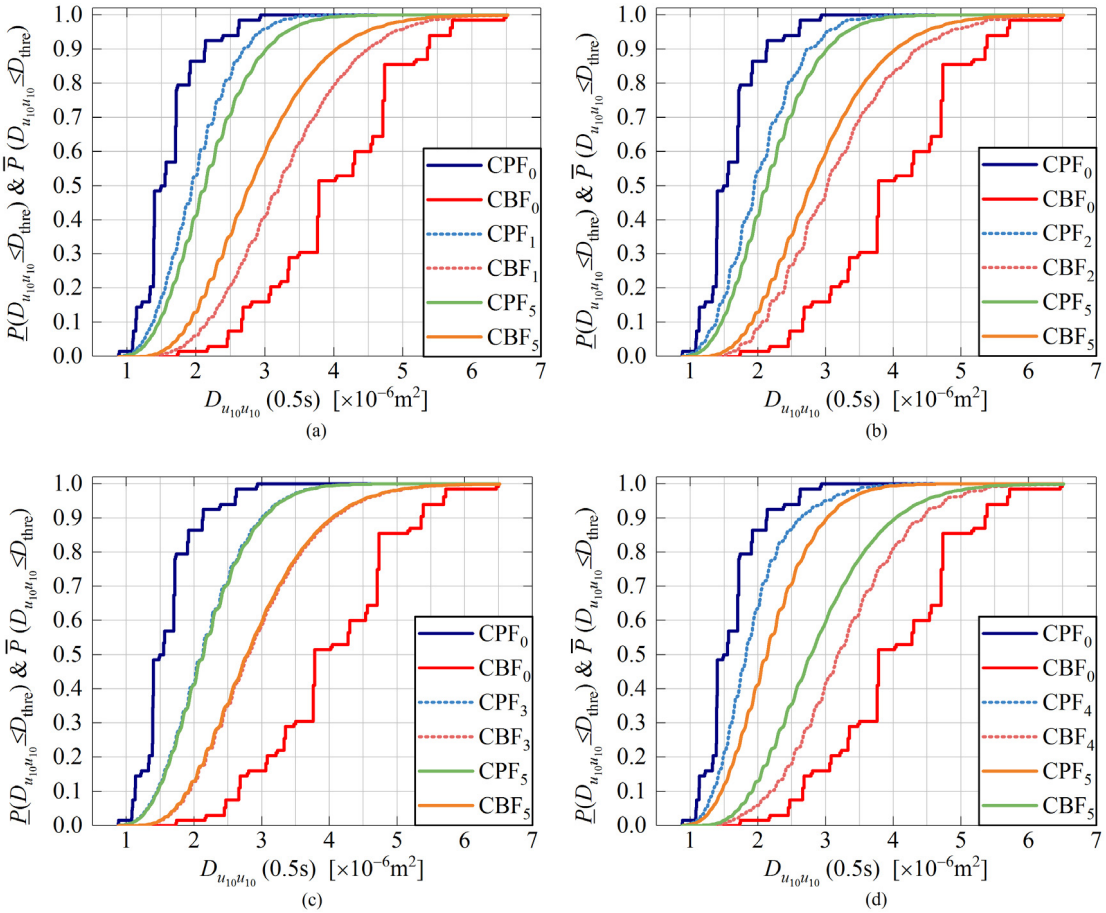

Fig. 13. Comparison of the cumulative distribution of $D_{u_{10}u_{10}}$(0.5 s) for different combinations of focal elements fixed by (a) the uncertain information of Young's modulus E, (b) the uncertain information of the cross section of the truss element A, (c) the uncertain information of material density ρ, and (d) the uncertain information of the lumped node mass M.

distances of the CPF$_0$ and CBF$_0$ curves, thereby demonstrating that epistemic uncertainty is gradually diminished because of the collection of uncertain information for each uncertain parameter. In particular, Fig. 13(c) shows that the cumulative curves obtained by fixing the material density of the truss element ρ coincide with the cumulative curves obtained by updating all the variables. This finding indicates that the epistemic uncertainty rooted in the material density of truss element ρ have minimal influence on the epistemic uncertainty associated with $D_{u_{10}u_{10}}$(0.5 s), and thus, can be ignored in the UQ process. That is, the epistemic uncertainty involved in the variation of $D_{u_{10}u_{10}}$(0.5 s) is mainly contributed by the variation of Young's modulus E, the cross section of the truss element A, and lumped node mass M. To validate the effectiveness of the proposed sensitivity analysis in the time evolution history, the $(D_{u_{10}u_{10}})^{0.5}$ is applied as shown in Fig. 14.

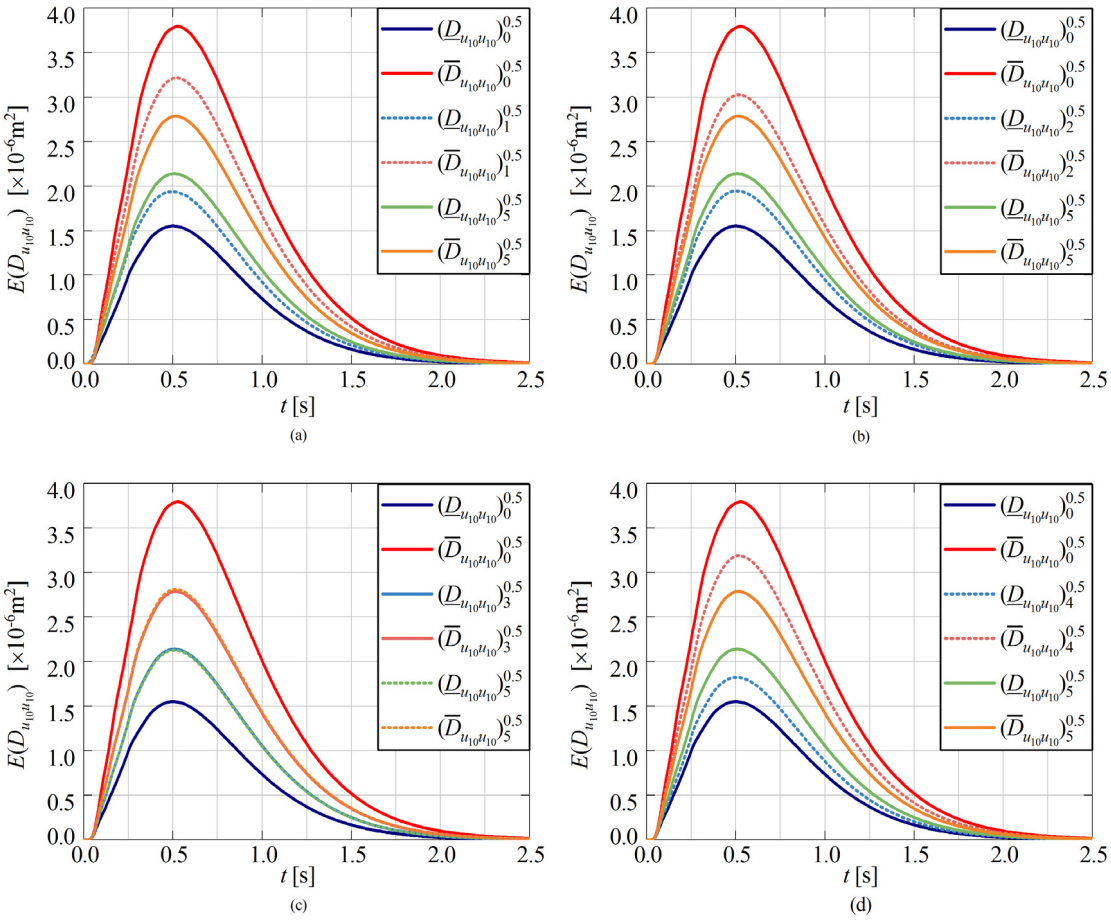

Fig. 14. Upper and lower bounds of the time history of $(D_{u_{10}u_{10}})^{0.5}$.

As shown in Fig. 14, the variation tendency of the enveloped area produced by different couplings of the CPF and CBF curves is consistent with the variation shown in Fig. 13. When the character of the linear system is considered, the variation of an enveloped area is fixed. Figs. 13 and 14 show that the material density of the truss element ρ is less important than uncertain parameters E, A, and M. On the basis of the sensitivity results of the proposed sensitivity analysis method, the proposed method is determined to be feasible and effective.

7. Conclusions

This work is presented to investigate the influence of structural epistemic uncertainty on structural dynamic response under stochastic excitation by introducing evidence theory into the UQ framework. Evidence theory is used to model epistemic uncertainties rooted in structural variables. To overcome the computational bottleneck of the evidential propagation process, an adaptive strategy is used in the sub-interval perturbation method using the first-order Taylor expansion series to evaluate the lower and upper bounds of system response by considering the exponential increment of the joint focal element in complex and large-scale engineering problems. The dimension of an uncertain system input is effectively reduced by applying sensitivity analysis. The cumulative distribution for the belief structure of system response is constructed to evaluate the uncertainty level in system response under stochastic excitation using the BCDF concept. Numerical examples illustrate that the UQ results obtained via ASPM exhibit more prominent convergence and accuracy compared with the results obtained via the classical SPM and MC simulation. Compared with the classical SPM, the calculation efficiency of the proposed ASPM evidently improves with a slight decrease in computational accuracy. The efficiency of the presented sensitivity analysis is also validated by comparing the epistemic involved in system response under sparse and abundant data.

Acknowledgments

This study was supported by the Ministry of Science and Technology of China (Grant No. SLDRCE14-B-03), the National Natural Science Foundation of China (Grant No. 51178337), and the Natural Science Foundation of Shanghai (Grant No. 17ZR1431900).

References

[1] W.L. Oberkampf, J.C. Helton, K. Sentz, Mathematical representation of uncertainty, in: Am. Inst. Aeronaut. Astronaut. Non-Deterministic Approaches Forum, Seattle, WA, 2001, pp. 1–23. http://dx.doi.org/10.2514/6.2001-1645.

[2] A. Der Kiureghian, O. Ditlevsen, Aleatory or epistemic? Does it matter?, Struct. Saf. 31 (2009) 105–112. http://dx.doi.org/10.1016/j.strusafe.2008.06.020.

[3] J. Lin, Y. Zhao, Y. Zhang, Accurate and highly efficient algorithms for structural stationary non-stationary random responses, Comput. Methods Appl. Mech. Engrg. 191 (2001) 9. http://dx.doi.org/10.1016/S0045-7825(01)00247-X.

[4] L.D. Lutes, S. Sarkani, Random Vibrations: Analysis of Structural and Mechanical Systems, Elsevier, Butterworth–Heinemann, Burlington, 2004.

[5] J. Lin, W. Zhang, F.W. Williams, Pseudo-excitation algorithm for nonstationary random seismic responses, Eng. Struct. 16 (1993) 270–276. http://dx.doi.org/10.1016/0141-0296(94)90067-1.

[6] C. Soize, Stochastic modeling of uncertainties in computational structural dynamics—Recent theoretical advances, J. Sound Vib. 332 (2013) 2379–2395. http://dx.doi.org/10.1016/j.jsv.2011.10.010.

[7] M. Shinozuka, Monte Carlo solution of structural dynamics, Comput. Struct. 2 (1972) 855–874. http://dx.doi.org/10.1016/0045-7949(72)90043-0.

[8] G. G. Roger, D. S. Pol, Stochastic Finite Elements: A Spectral Approach, first ed., Dover Publiacations, Inc, New York, 2003.

[9] L. Jie, S. Liao, Response analysis of stochastic parameter structures under non-stationary random excitation, Conmput. Mech. 27 (2001) 8. http://dx.doi.org/10.1142/S0219876206000771.
[10] W.K. Liu, T.B.E.L. Ytschko, A. Mani, Probabilistic finite elements for nonlinear structural dynamics, Comput. Methods Appl. Mech. Engrg. 56 (1986) 61–81. http://dx.doi.org/10.1016/0045-7825(86)90136-2.
[11] F. Wu, W.X. Zhong, A hybrid approach for the time domain analysis of linear stochastic structures, Comput. Methods Appl. Mech. Engrg. 265 (2013) 71–82. http://dx.doi.org/10.1016/j.cma.2013.06.006.
[12] J. Li, J.-B. Chen, Dynamic response and reliability analysis of structures with uncertain parameters, Internat. J. Numer. Methods Engrg. 62 (2005) 289–315. http://dx.doi.org/10.1002/nme.1204.
[13] W. Gao, N.J. Kessissoglou, Dynamic response analysis of stochastic truss structures under non-stationary random excitation using the random factor method, Comput. Methods Appl. Mech. Engrg. 196 (2007) 2765–2773. http://dx.doi.org/10.1016/j.cma.2007.02.005.
[14] V. Papadopoulos, O. Kokkinos, Variability response functions for stochastic systems under dynamic excitations, Probab. Eng. Mech. 28 (2012) 176–184. http://dx.doi.org/10.1016/j.probengmech.2011.08.002.
[15] V. Papadopoulos, O. Kokkinos, Transient response of stochastic finite element systems using dynamic variability response functions, Struct. Saf. 52 (2015) 100–112. http://dx.doi.org/10.1016/j.strusafe.2014.09.006.
[16] L.A. Zadeh, Fuzzy sets, Inf. Control 8 (1965) 338–353. http://dx.doi.org/10.1016/S0019-9958(65)90241-X.
[17] D. Dubois, H.M. Prade, H. Farreny, R. Martin-Clouaire, C. Testemale, Possibility Theory: An Approach to Computerized Processing of Uncertainty, Plenum press, New York, 1988.
[18] R.E. Moore, Interval Analysis, Prentice-Hall, Englewood Cliffs, 1966.
[19] P. Walley, Statistical Reasoning with Imprecise Probabilities, Chapman and Hall, London, 1991.
[20] A.P. Dempster, Upper and lower probabilities induced by a multivalued mapping, Ann. Math. Stat. 38 (1967) 325–339.
[21] G. Shafer, A Mathematical Theory of Evidence, Princeton University Press, Princeton, 1976.
[22] G.J. Klir, R.M. Smith, On measuring uncertainty and uncertainty-based information: recent developments, Ann. Math. Artif. Intell. 32 (2001) 5–33. http://dx.doi.org/10.1023/A:1016784627561.
[23] S. Huang, X. Su, Y. Hu, S. Mahadevan, Y. Deng, A new decision-making method by incomplete preferences based on evidence distance, Knowl.-Based Syst. 56 (2014) 264–272. http://dx.doi.org/10.1016/j.knosys.2013.11.019.
[24] H.-R. Bae, R.V. Grandhi, R.A. Canfield, An approximation approach for uncertainty quantification using evidence theory, Reliab. Eng. Syst. Saf. 86 (2004) 215–225. http://dx.doi.org/10.1016/j.ress.2004.01.011.
[25] J.C. Helton, J.D. Johnson, W.L. Oberkampf, C.B. Storlie, A sampling-based computational strategy for the representation of epistemic uncertainty in model predictions with evidence theory, Comput. Methods Appl. Mech. Engrg. 196 (2007) 3980–3998. http://dx.doi.org/10.1016/j.cma.2006.10.049.
[26] S. Salehghaffari, M. Rais-Rohani, E.B. Marin, D.J. Bammann, A new approach for determination of material constants of internal state variable based plasticity models and their uncertainty quantification, Comput. Mater. Sci. 55 (2012) 237–244. http://dx.doi.org/10.1016/j.commatsci.2011.11.035.
[27] H. Tang, Y. Su, J. Wang, Evidence theory and differential evolution based uncertainty quantification for buckling load of semi-rigid jointed frames, Sadhana 40 (2015) 1611–1627. http://dx.doi.org/10.1007/s12046-015-0388-0.
[28] H. Shah, S. Hosder, T. Winter, Quantification of margins and mixed uncertainties using evidence theory and stochastic expansions, Reliab. Eng. Syst. Saf. 138 (2015) 59–72. http://dx.doi.org/10.1016/j.ress.2015.01.012.
[29] Z. Qiu, X. Wang, Parameter perturbation method for dynamic responses of structures with uncertain-but-bounded parameters based on interval analysis, Int. J. Solids Struct. 42 (2005) 4958–4970. http://dx.doi.org/10.1016/j.ijsolstr.2005.02.023.
[30] Z. Qiu, X. Wang, Comparison of dynamic response of structures with uncertain-but-bounded parameters using non-probabilistic interval analysis method and probabilistic approach, Int. J. Solids Struct. 40 (2003) 5423–5439. http://dx.doi.org/10.1016/S0020-7683(03)00282-8.
[31] M.V. Rama Rao, A. Pownuk, S. Vandewalle, D. Moens, Transient response of structures with uncertain structural parameters, Struct. Saf. 32 (2010) 449–460. http://dx.doi.org/10.1016/j.strusafe.2010.05.001.
[32] G. Muscolino, A. Sofi, Response statistics of linear structures with uncertain-but-bounded parameters under gaussian stochastic input, Int. J. Struct. Stab. Dyn. 11 (2011) 775–804. http://dx.doi.org/10.1142/s0219455411004348.
[33] G. Muscolino, A. Sofi, Stochastic analysis of structures with uncertain-but-bounded parameters via improved interval analysis, Probab. Eng. Mech. 28 (2012) 152–163. http://dx.doi.org/10.1016/j.probengmech.2011.08.011.
[34] Z. Qiu, I. Elishakoff, Antioptimization of structures with large uncertain-but-non-random parameters via interval analysis, Comput. Methods Appl. Mech. Engrg. 152 (1998) 12. http://dx.doi.org/10.1016/S0045-7825(96)01211-X.
[35] Y.T. Zhou, C. Jiang, X. Han, Interval and subinterval analysis methods of the structural analysis and their error estimations, Int. J. Comput. Methods 3 (2006) 229–244. http://dx.doi.org/10.1142/S0219876206000771.
[36] B. Xia, D. Yu, Modified interval and subinterval perturbation methods for the static response analysis of structures with interval parameters, J. Struct. Eng. 140 (2014) 4013113. http://dx.doi.org/10.1061/(asce)st.1943-541x.0000936.
[37] B. Xia, D. Yu, J. Liu, Interval and subinterval perturbation methods for a structural-acoustic system with interval parameters, J. Fluids Struct. 38 (2013) 146–163. http://dx.doi.org/10.1016/j.jfluidstructs.2012.12.003.
[38] C. Wang, Z. Qiu, Subinterval perturbation methods for uncertain temperature field prediction with large fuzzy parameters, Int. J. Therm. Sci. 100 (2016) 381–390. http://dx.doi.org/10.1016/j.ijthermalsci.2015.10.013.
[39] S. Yin, D. Yu, H. Yin, H. Lü, B. Xia, Hybrid evidence theory-based finite element/statistical energy analysis method for mid-frequency analysis of built-up systems with epistemic uncertainties, Mech. Syst. Signal Process. 93 (2017) 204–224. http://dx.doi.org/10.1016/j.ymssp.2017.02.001.
[40] R.R. Yager, Cumulative distribution functions from dempster-shafer belief structures, IEEE Trans. Syst. Man Cybern. B 34 (2004) 2080–2087. http://dx.doi.org/10.1109/tsmcb.2004.833772.
[41] F. Durante, J. Fernández Sánchez, W. Trutschnig, On the interrelation between Dempster–Shafer belief structures and their belief cumulative distribution functions, Knowl.-Based Syst. 52 (2013) 107–113. http://dx.doi.org/10.1016/j.knosys.2013.07.012.
[42] C. Jiang, B. Wang, Z.R. Li, X. Han, D.J. Yu, An evidence-theory model considering dependence among parameters and its application in structural reliability analysis, Eng. Struct. 57 (2013) 12–22. http://dx.doi.org/10.1016/j.engstruct.2013.08.028.
[43] L. Xie, J. Liu, J. Zhang, X. Man, Evidence-theory-based analysis for structural-acoustic field with epistemic uncertainties, Int. J. Comput. Methods (2016) 1750012. http://dx.doi.org/10.1142/s0219876217500128.
[44] H. Tang, D. Li, J. Li, S. Xue, Epistemic uncertainty quantification in metal fatigue crack growth analysis using evidence theory, Int. J. Fatigue 99 (Part 1) (2017) 163–174. http://dx.doi.org/10.1016/j.ijfatigue.2017.03.004.